RESEARCH ARTICLE

Analysis of impact dynamics and deposition of single and multiple PEDOT:PSS solution droplets

Dominikus Brian[1] · Morteza Eslamian[1]

Abstract

In line with recent efforts and developments in emerging printed electronics, using solution-processed coatings, we studied the impact dynamics and deposition of single and multiple polymeric aqueous and isopropanol (IPA)-diluted PEDOT:PSS solution droplets, across seven orders of magnitude timescale. The solution properties and release height of droplets from a needle were varied to generate Weber numbers in the range of 94–510, with two Ohnesorge numbers of 0.0108 and 0.0195, for aqueous and IPA-diluted PEDOT:PSS solution droplets, respectively. The former droplet on FTO glass substrate is partially wetting, whereas the latter is fully wetting, generating different phenomena in the prolonged wetting and drying time. The solutions showed shear-thinning behavior at high shear rates, but viscosity immediately reached a saturated limit at higher shear rates and, therefore, the fluids behaved as Newtonian fluids during impact. Among the results, the addition of IPA resulted in improved spreading of PEDOT:PSS in the wetting phase, with wetting trend following the Tanner's law. We then assessed the prediction power of existing models to predict maximum spreading, taking into account the role of measured static and dynamic contact angles during spreading. Multiple droplets (2, 5, and 15) were impacted nearly simultaneously and formed lines and films. We examined the bridge formation, spreading length growth, and shape evolution of multiple coalescing droplets. We also correlated the formed surface area with the number of coalescing droplets and discussed the ideality of the shape of the formed film. The results of this study will help to pave the way for large-scale manufacturing of organic coatings using droplet-based methods.

Graphic abstract
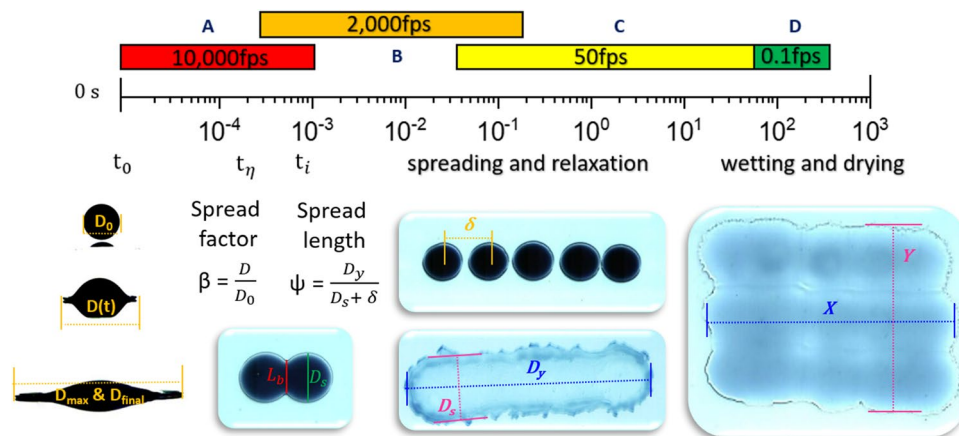
Extended author information available on the last page of the article

1 Introduction

Today, organic thin films are ubiquitous in the fabrication of photonic and optoelectronics devices, such as TV and mobile phone displays, sensors, and other thin film devices (Ouyang et al. 2005; Eslamian 2017). However, currently such thin film coatings are typically deposited by thermal evaporation, which is a physical vapor deposition technique and entails high energy for vaporizing the precursors in sophisticated and expensive vacuum chambers and in a batch process, resulting in substantial cost of the final products. Solution-based deposition methods, either droplet-based or liquid-film-based approaches, are believed to be a low-cost alternative to vapor-phase methods, given that they use less expensive equipment and processes performed in atmospheric conditions. Droplet-based fabrication routes including inkjet printing (Wijshoff 2018), spray coating (Eslamian 2013, 2014), aerosol jet printing (Mahajan et al. 2013), and simple drop-casting or multiple-droplet drop-casting (MDDC) (Eslamian and Soltani-Kordshuli 2018) all work based on impingement of a single or multiple droplets on a targeted substrate to gradually form a thin film coating.

The intricate physics and fluid dynamics of droplet-based techniques are still partially understood, as discussed in a recent review (Wijshoff 2018) and references therein. There are still challenges to address to adapt the aforementioned droplet-based methods for printing/coating a diverse range of advanced materials with high resolution and minimum defects. In this context, here we performed an in-depth study of the impact, spreading, coalescence, and pattern formation of multiple aqueous and isopropanol (IPA)-diluted poly(3,4-ethylenedioxythiophene): poly(styrene sulfonate) (PEDOT:PSS) droplets, a widely used organic material. PEDOT:PSS is a precursor solution used as the ink for deposition and printing of conducting polymeric films (Elschner et al. 2010; Zabihi et al. 2015), thin film solar cells (Eom et al. 2009), and temperature sensors (Rivadeneyra et al. 2019), to name a few.

Droplet impact dynamics is a topic that has been extensively studied, e.g., (Scheller and Bousfield 1995; Pasandideh-Fard et al. 1996; Rioboo et al. 2001; Biance et al. 2004; Roisman 2009; Roisman et al. 2009; Eggers et al. 2010; Antonini et al. 2012), as reviewed by Yarin (2006) and (Pasandideh-Fard et al. 1996; Biance et al. 2004; Roisman 2009; Roisman et al. 2009) Josserand and Thoroddsen (2016). Most studies, however, concern the initial and early stage of the phenomena and deal with simple Newtonian liquids. Studies on single droplet impact of complex liquids are also available such as the effect of substrate vibrations and surface energy on spreading of PEDOT:PSS droplets (Soltani-Kordshuli and Eslamian 2017), impact

and spreading of perovskite solution droplets (Brian et al. 2019), non-Newtonian liquids (Cooper-White et al. 2002; Bartolo et al. 2007; German and Bertola 2009; Bertola 2013; Laan et al. 2014), and edible coating formulations (Andrade et al. 2015), to name a few.

When more than one droplets are deposited in the vicinity of each other, they may establish contact due to kinetic energy or attractive long-range forces between the droplets (Cira et al. 2015). At the point of contact, a curvature/neck/bridge forms, the length of this bridge, L_b, then will grow with time, t. In general, one expects to observe a scaling law in the form $L_b \propto t^{1/2}$, in the inertia-driven regime (Eggers et al. 1999; Duchemin et al. 2003), a linear scaling $L_b \propto t$, in the viscous-driven coalescence (Paulsen et al. 2011), and $L_b \propto t^{1/4}$, in a viscous system in the partially wetting phase. For simple liquids, studies have been carried out to understand the early hydrodynamics (Eggers et al. 1999; Aarts et al. 2005; Thoroddsen et al. 2007), the subsequent spreading (Ristenpart et al. 2006), interplay of viscosity and inertia (Paulsen et al. 2011), influence of surface tension (Menchaca-Rocha et al. 2001; Wu et al. 2004), effect of contact line dynamics (Narhe et al. 2004), viscous shear stresses due to substrate (Lee et al. 2012), substrate porosity (Yarin et al. 2019), geometrical factors (Hernández-Sánchez et al. 2012; Eddi et al. 2013), speed of the process (Thoroddsen et al. 2005), and the long-term relaxation (Andrieu et al. 2002).

For complex liquids with two or more droplets simultaneously or sequentially impacted onto a surface with a time lag, some studies have been performed, e.g., (Li et al. 2010; Castrejón-Pita et al. 2013; Sarojini et al. 2016; Ashoke Raman et al. 2017; Eslamian and Soltani-Kordshuli 2018). For line and pattern formation, few works have been carried out, where concern was only with the final state of the line or film (Duineveld 2003; Lee et al. 2013; Wijshoff 2018). To fabricate a thin film coating using drop-based methods, understanding the wetting and evolution dynamics across the intermediate and longer timescales is essential. Therefore, this study was designed and conducted to span across seven orders of magnitude of timescale—from 0.0001 to 300 s. To this end, firstly, we established the analytical ground by studying the impact and spreading dynamic of a single PEDOT:PSS droplet, utilizing existing prediction models (Chandra and Avedisian 1991; Pasandideh-Fard et al. 1996; Mao et al. 1997; Clanet et al. 2004; Ukiwe and Kwok 2005; Roisman et al. 2009; Laan et al. 2014). Secondly, we investigated the coalescence and film formation of two and five droplets deposited in a linear array. Thirdly, we studied the scaling of a number of droplets with its yielded area, involving as many as 15 droplets.

2 Theoretical framework

Throughout the impact of a small droplet on a solid substrate, assuming negligible effect of gravity and surrounding air, there are three main forces that should be accounted for: inertia, viscous, and capillary forces. The interplay between these forces can be expressed by Reynolds number, $Re = \rho D_0 U_0 / \eta$, where ρ is the density, D_0 is the droplet initial diameter, U_0 is the impact velocity, and η is the dynamic viscosity, Weber number, $We = \rho D_0 U_0^2 / \sigma$, where σ is the surface tension of the liquid, and Ohnesorge number, $Oh = We^{0.5}/Re$. When a droplet impinges with a substrate, spreading and wetting take place. A spreading parameter $S = \sigma_{sv} - (\sigma + \sigma_{sl})$ is defined based on the interfacial tensions (De Gennes 1985), where σ_{sv} and σ_{sl} are the solid–vapor and solid–liquid interfacial tensions, respectively. If $S \geq 0$, we expect the system to spread completely, so as to minimize the energy of the system.

To begin with, we assess the spreading dynamic of single droplet impact based on three approaches: (1) energy conservation (Chandra and Avedisian 1991), (2) mass-momentum conservation (Pasandideh-Fard et al. 1996; Mao et al. 1997; Clanet et al. 2004; Ukiwe and Kwok 2005; Roisman et al. 2009), and (3) a more recent approach that balances the two (Eggers et al. 2010; Laan et al. 2014). In their simplest forms, in approach (1), the spread ratio, $\beta = D/D_0$ is correlated with $We^{0.5}$, where D is the spread diameter. In approach (2), β is correlated with $We^{0.25}$, while in approach (3), β is correlated with $We\,Re^{-0.4}$.

The energy conservation approach (1) postulates that energy contained within the droplet prior to impact is equal to the sum of all energies after the impact. That is $E_k + E_p + E_S = E_S' + E_p' + E_{vis}$, where the kinetic energy, $E_k = \frac{1}{2}\rho U_0^2 \left(\frac{\pi}{6} D_0^3\right)$, the potential energy, $E_p = \rho\left(\frac{\pi}{6} D_0^3\right) g \frac{D_0}{2}$, the surface energy prior to impact, $E_S = \pi D_0^2 \sigma_{lv}$, the surface energy at maximum spreading (D_{max}), $E_S' = \frac{\pi}{4}\sigma_{lv}(1 - \cos\theta)D_{max}^2$, and the viscous dissipation $E_{vis} = \frac{\pi}{3}\rho U^2 D_0 D_{max}^2 \frac{1}{\sqrt{Re}}$. Noting that $E_p \cong E_p'$, and its contribution relative to the inertia is small, E_p and E_p' are, therefore, comparable and dropped. Hence, we are left with $E_k + E_S = E_S' + E_{vis}$. Plugging in all the components into the energy conservation equation and rearrange them based on the We and Re definitions, one can obtain scaling laws for β_{max} of the form $We^{0.5}$, $We^{0.25}$, $Re^{0.2}$, and $Re^{0.25}$, depending on the assumptions and simplification imposed. One such equation was derived by Chandra and Avedisian (1991), shown as Eq. S1 of the supplementary information (SI).

Approach (2) implies that one can predict the final form of the droplet by assuming that its momentum is converted into droplet motion. This approach, however, often requires additional information such as total spreading time, the thickness of the lamella, or spreading velocity, which take a

general form such as Eq. S2 of the SI. To account for wettability effect, Ukiwe and Kwok (2005) proposed modification by means of using different contact angles arriving at Eq. S3 of the SI. However, using quasi-static or dynamic contact angles will yield different prediction of β_{max} (Fukai et al. 1995). Further, Mao et al. (1997) included the thickness of the formed boundary layer and derived Eq. S4, shown in the SI. Roisman et al. (2009) developed a model that attempts to increase universality by assessing various flow characteristic parameters, Eq. S5 of the SI. All the above models have a dependency on We number. Clanet et al. (2004) proposed a simple but effective semi-empirical correlation in the form $\beta_{max} = 0.9We^{0.25}$, Eq. S6 of the SI.

The more recent approach (3) considers all forces. One recent model of this type was proposed by Laan et al. (2014) in the form of $\beta_{max} = Re^{0.2}\frac{P^{0.5}}{A + P^{0.5}}$, Eq. S7 of the SI, where $P = WeRe^{-0.25}$ is the impact number and A is a matching coefficient, with proposed universal value of 1.24 ± 0.01, for a wide range of We and Re numbers.

3 Experimental

3.1 Materials

Pristine aqueous PEDOT:PSS solution with concentration of 1.3 wt% (Clevios PH1000, Heraeus, Germany) was purchased through Xi'an Polymer Co., China. In this product, the mass ratio of PEDOT to PSS components is 1:2.5, where the PEDOT:PSS particles with size of ~25 nm were dispersed in water, hereafter referred to as aqueous PEDOT:PSS. Prior to each experiment, the PEDOT:PSS solution was first filtered using PVDF filter with pore size of 0.45 μm. The filtered solution was then ultrasonicated for a duration of 30 min. The isopropanol (IPA)-diluted PEDOT:PSS was prepared by further dilution of aqueous PEDOT:PSS with aqueous PEDOT:PSS to IPA volume ratio of 1:2. After mixing, the IPA-diluted PEDOT:PSS was again filtered and ultrasonicated for 30 min.

The substrate used in this study is a smooth 10 cm × 10 cm fluorine tin-oxide (FTO)-coated glass, commonly used in thin film devices. The roughness of FTO glass used here is ~46 nm, measured by a surface profilometer (KLA-Tencor P7, USA), where details were reported elsewhere (Eslamian and Soltani-Kordshuli 2018). Prior to usage, the substrate was cleaned and UV treated to ensure chemical homogeneity and to enhance its surface energy. The cleaning was done by sonicating the substrates first in water bath, then IPA, and followed by acetone for 10 min, at each stage. The cleaned substrate was further treated in a UV–ozone furnace for 15 min.

3.2 Methods

The setup for this study is composed of droplet generation and image acquisition systems (Fig. 1). The droplets were generated using a multi-channel microliter pipettor (DragonLab, China), equipped with capillary tips with an inner diameter of 0.41 mm (G22), and 10 mm spacing between its tips. The dispensed liquid volume per droplet is 18 μl ($D_0 = 3.29 \pm 0.06$ mm) and 9 μl ($D_0 = 2.57 \pm 0.16$ mm) for the aqueous and IPA-diluted PEDOT:PSS droplets, respectively. To obtain a range of impact velocities, the capillary tube tip was vertically adjusted to a height 10, 20, and 30 cm above the substrate, corresponding to impact velocity of 1.40, 1.98, and 2.42 m/s, respectively. A CMOS color high-speed camera (Photron SA3 120-C, Japan) was employed for image acquisition. Cross-sectional and top surface images were acquired at 10,000 and 2000 frames per second (fps), respectively. The slow wetting processes were also captured at 50 and then 0.1 fps. The aforementioned modes hereafter designated as mode A, B, C, and D, respectively, as shown in Fig. 1.

Acquired images were post-processed using ImageJ software. The negative influences of sources of uncertainty were minimized by extra steps such as using disposable syringe tip, precise volume dispensing, placing airflow shield box surrounding the experiment zone, and ensuring back pressure nullification. The experimental drop size, lamella diameter, and other extracted geometrical data are reproducible with variation between 2 and 6%.

3.3 Characterization

Density was measured by weighing five samples (Mettler Toledo, ME 104, USA) with exact volume of the solution inside a precision microliter glass cell. Rheological data were obtained by a parallel plate rotational rheometer (Anton Paar MCR 302, USA), using a 0.5 mm gap, with shear rate, γ, ranging from 0.1 to 1000 s^{-1}, shown in Fig. 2.

Pendant droplet method was used to measure surface tension by a tensiometer (Theta, Biolin Scientific, Finland). Static contact angle values were acquired by sessile droplet method. Advancing and receding contact angle experiments
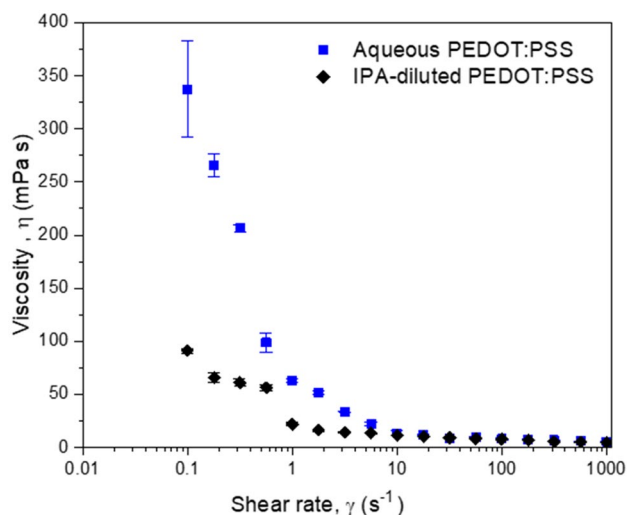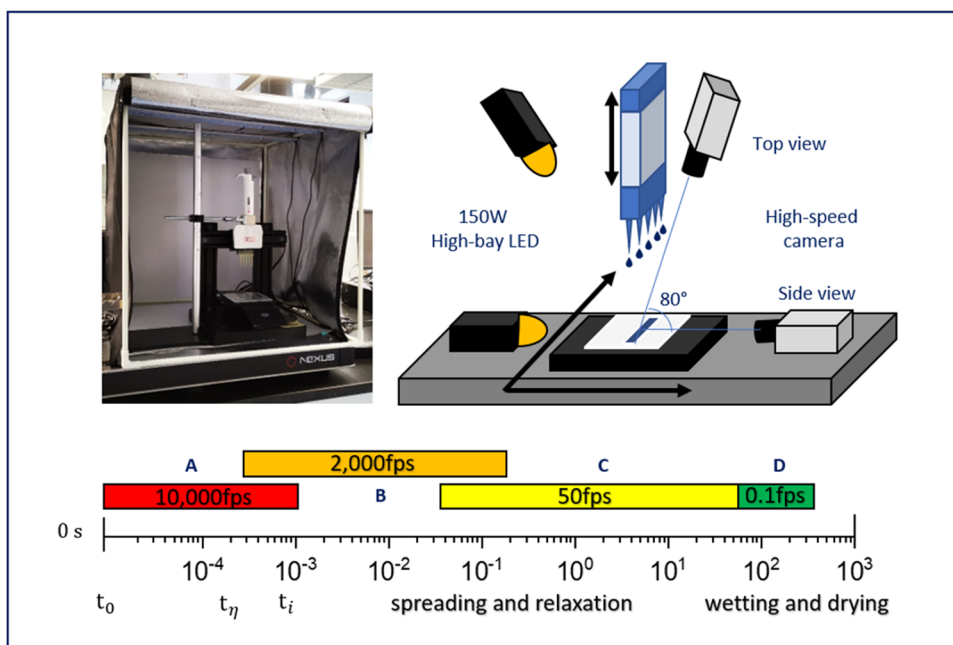
Fig. 2 Viscosity versus the shear rate of aqueous and IPA-diluted PEDOT:PSS measured at 23 °C

Fig. 1 Schematic depicting the imaging setup (right) and a photograph of the experimental stage (left)

Table 1 Measured density (ρ), infinite shear viscosity (η), and liquid–vapor surface tension (σ) of mixtures used in this work

Solution	ρ (g/ml)	η (mPa·s)	σ (mN/m)
Aqueous PEDOT:PSS	1.012 ± 0.05	5.22 ± 0.13	69.66 ± 2.71
IPA-diluted PEDOT:PSS	0.840 ± 0.2	4.50 ± 0.08	24.79 ± 1.02

Table 2 Parameters associated with the shear-thinning degree of the PEDOT:PSS solutions

Solution	K (mPa)	n (–)	R^2
Aqueous PEDOT:PSS	1.7974 ± 0.0097	0.5324 ± 0.0076	0.9294
IPA-diluted PEDOT:PSS	1.3413 ± 0.0285	0.6824 ± 0.0028	0.9245

were measured by drop-running-on-the-hill method, with base tilting angle of 45°. Image analysis for surface tension and static, advancing, and receding contact angle measurements was performed by the tensiometer built-in analysis software (Attension, Biolin Scientific, Finland). Dynamic contact angles were measured from the cross-sectional images of the spreading droplet recorded at 10,000 fps, using contact angle plug-in of ImageJ software. Surface energy of the substrate was determined by the classic two-liquid OWRK method, where deionized water (W) and diiodomethane (DI) (Macklin, USA) were used as the polar and dispersive probe liquids, respectively. The temperature of experimental enclosure box was 22 °C ± 1 °C, and relative humidity was 55% ± 5%. Liquid properties were obtained under the same environmental condition and are listed in Table 1.

To characterize the quantitative degree of shear-thinning of PEDOT:PSS solutions, the rheological measurements, shown in Fig. 2, were fitted by the power law model, using the following equation:

$$\eta_{\text{eff}} = K\gamma^{n-1}, \tag{1}$$

where η_{eff} is the effective viscosity, γ is the shear rate, K is the consistency coefficient, and n is the power law index. By least square curve fitting, the corresponding K and n values were calculated and listed in Table 2.

Through monitoring the growth of lamella diameter over time, $D(t)$, we could track the velocity of the contact line, U_{cl} using high-speed images. At time ~ 0.1 ms, the U_{cl} is ~ 6–9 m/s and ~ 5–7 m/s for aqueous and IPA-diluted PEDOT:PSS, respectively. At 2–3 ms, U_{cl} slows down to ~ 1 m/s and eventually approaches zero at the end of the process. The shear rate in s^{-1} at a given time interval Δt is proportional to $\frac{U_{\text{cl}}}{D(t+\Delta t)-D(t)}$ from a dimensional analysis. From the above reasoning, we deduce a shear rate as high as ~ 10^4–10^5 s^{-1}, occurring throughout the spreading process. Considering the viscosity measurements of Fig. 2, as soon as shear rate increases, the viscosity of both PEDOT:PSS solutions decreases considerably and remains constant. Therefore, the spreading behavior of both solutions studied here is Newtonian with viscosity $\eta = \eta_\infty$, listed in Table 1. Using this viscosity, the dimensionless numbers are given in Table 3, where the 6 basic single droplet cases generate Re numbers ranging from 671 to 1544, and We numbers ranging from 94 to 510. $K = WeOh^{-0.4}$ is the splashing number to be discussed later.

4 Results and discussion

4.1 Surface energy and impact regime map

Surface energy of the substrate affects spreading state of a droplet impinged upon it. The measured data of FTO-coated glass and a microscope glass slide, for comparison, are listed in Table 4. The surface energy of the FTO-coated glass is large and well within the category of hydrophilic substrates, with water contact angle of ~ 20°. Carrying out a 15-min UV treatment yielded further increase in the substrate total surface energy from 70.81 to 80.09 mN/m, where such increase of surface energy was previously reported for other complex substrates (Brian et al. 2019). We found that the main contributor to this increase is of London dispersive origin.

Following Schiaffino and Sonin (1997), we plotted our dimensionless numbers into an impact regime map as shown in Fig. 3. In the map, region A is based on the typical conditions of spray coating process, as discussed by Eslamian (2013), with $U_0 = 1$–10 m/s and $D_0 = $ ~ 10–200 μm. Our data

Table 3 Dimensionless numbers of experimental cases investigated in this study

Solution	D_0 (mm)	U_0 (m/s)	Re	We	$K = We\,Oh^{-0.4}$	Oh
Aqueous PEDOT:PSS	3.29 ± 0.06	1.40	893	94	572	0.0108
		1.98	1262	187	1144	
		2.42	1544	280	1710	
IPA-diluted PEDOT:PSS	2.57 ± 0.16	1.40	672	171	825	0.0195
		1.98	950	341	1651	
		2.42	1161	510	2466	

Table 4 Polar, dispersive, and total surface free energy ($\sigma_{sv}^{p}, \sigma_{sv}^{d}, \sigma_{sv}$), respectively, of FTO-coated substrate, used in this study and microscope glass slide as a reference substrate

Substrate	Condition	σ_{sv} (mN/m)	σ_{sv}^{p} (mN/m)	σ_{sv}^{d} (mN/m)	θ_w (°)	θ_{DI} (°)
FTO-coated glass	As-received	70.81 ± 1.51	39.01 ± 3.19	31.81 ± 4.69	18.95 ± 0.783	54.24 ± 10.19
	UV-cured	80.09 ± 0.11	33.65 ± 0.11	48.22 ± 0.22	3.34 ± 0.08	18.44 ± 0.99
Microscope glass slide	As-received	67.60 ± 2.16	32.75 ± 0.94	35.149 ± 3.09	28.61 ± 2.56	48.3 ± 6.92
	UV-treated	79.06 ± 0.14	33.06 ± 0.15	45.90 ± 0.29	2.73 ± 0.28	25.68 ± 1.00

θ_w is static contact angle of water, and θ_{DI} is static contact angle of diiodomethane

Fig. 3 Impact regime map in terms of *We* and *Oh* numbers. Region A denotes conditions typical of the spray coating process and Region B is the stable inkjet-based droplet-on-demand (DOD). Additional data points associated with the droplet impact of emerging materials are also shown. For sources of data points, see the main text
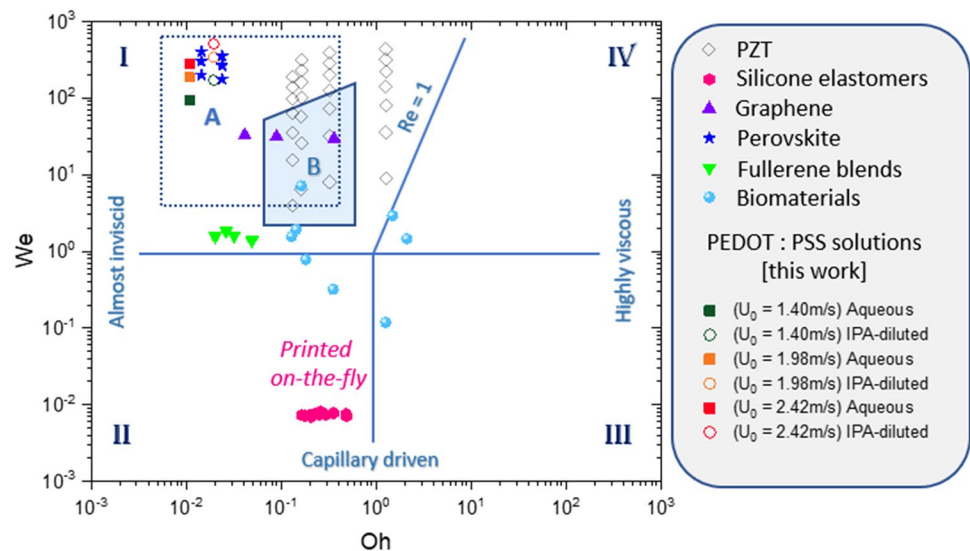

points fall in this region. Region B is associated with the stable inkjet-based droplet-on-demand (DOD) (Derby 2010). Additional data points associated with the droplet impact of emerging materials are also shown. When not stated either explicitly or implicitly in the references, it was assumed that $D_0 = 50$ μm and $U_0 = 1$ m/s, based on the standard droplet size and its corresponding droplet velocity of most commercial inkjet printers. Although some literature data points, such as for biomaterials, laid outside the so-defined "ideal zone" of conventional inkjet printing, they still showed a good printing outcome. One interesting technique is the printing on-the-fly (McCoul et al. 2017), where the droplet is captured by the substrate right during its initial flight, instead of the status quo printing. The PEDOT:PSS solutions are shear thinning at low shear rates, that is desired for inkjet printing, as it eases the jetting process and can be exploited to suppress secondary droplet formation during jetting (Hoath et al. 2012). The map also shows that droplets in our experiments are dominantly inertia driven (i.e., the data fall in regime I of Fig. 3). However, at later times when inertia and viscous forces have largely damped out, we expect wetting to play a more important role. Besides the role of *We* and *Oh* numbers, other complexity of specific solutions cannot be overlooked. Such complexities include

but are not limited to non-Newtonian rheology (German and Bertola 2009; Finotello et al. 2018), strong polar interaction of ionic solutions, as in perovskite solutions (Brian et al. 2019), aggregation of particles as in the fullerene blends (Hoth et al. 2007) and graphene solutions (Torrisi et al. 2012), phase change and drying, as with lead zirconate titanate (PZT) (Wang and Derby 2005) or silicone elastomers (McCoul et al. 2017), and printing with biomaterials (Gudapati et al. 2016).

4.2 Impact dynamics of a single droplet

4.2.1 General observations

During droplet impact on a hydrophilic, smooth solid substrate under atmospheric pressure, several phenomena may occur, such as air entrapment between the substrate and droplet, spreading with or without splashing, fingering and possible liquid lift-off and crown (corona) formation, receding, contact line depinning and retraction, followed by additional wetting. Qualitatively, the typical impact, spreading, and wetting dynamics of the two solutions used in this study are shown in Fig. 4 and additional images are provided in Figures S1 to S4 of the SI. As the figure shows, for aqueous
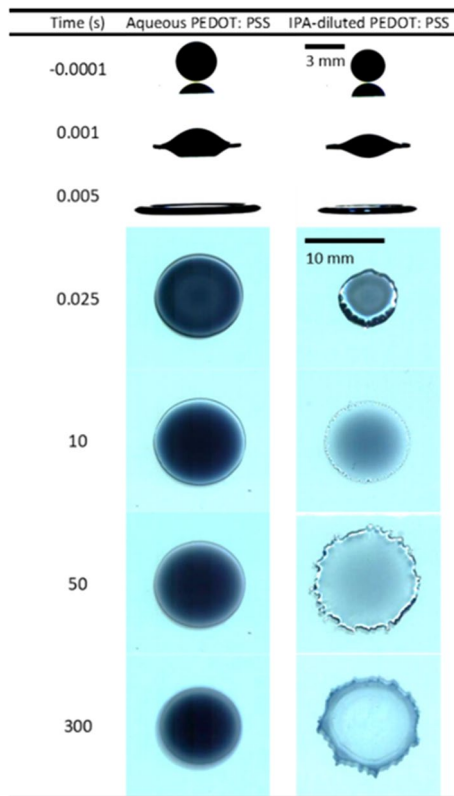
Fig. 4 Typical spreading process of aqueous (left column, $Re = 1544$, $We = 280$) and IPA-diluted (right column, $Re = 672$, $We = 171$) PEDOT:PSS droplets, using side and top view images

PEDOT:PSS solution droplet, the Re and We numbers are considerably larger than those of IPA-diluted PEDOT:PSS droplet. Consequently, at the early rapid kinematic stage, the aqueous PEDOT:PSS droplet spreads faster, but later, during pure wetting, the role of surface energy from the substrate kicks in, giving rise to significant increase in the spread size. We discussed various wetting phenomena observed in Sect. 4.2.3. In spreading stage, the aqueous PEDOT:PSS droplet deposits smoothly, with some level of receding and retraction. The IPA-diluted PEDOT:PSS droplet deposits followed by instabilities in the form of finger formation around the rim. For a surface tension dominant liquid, it has been argued that the origin of instability might be the Kelvin–Helmholtz instabilities due to an entrapped thin air film under the droplet (Liu et al. 2015). Yet, the initial rupturing at the rim might also be affected by the Plateau–Rayleigh instabilities (Thoroddsen and Sakakibara 1998; Xu 2010; Liu et al. 2015). For a viscous dominant liquid, the definite origin of such instability is still an open question. This instability would eventually drive the formation of capillary waves (Yarin and Weiss 1995; Thoroddsen and Sakakibara 1998; Rein and Delplanque 2008) that manifests itself in the form of fingering patterns, acted on the perimeter of the

initially stable rim. We noticed that the number and sizes of the fingers generated in the IPA-diluted PEDOT:PSS vary with time. The variation can be characterized by splitting and merging behavior of fingers discussed by Marmanis and Thoroddsen (1996) and Thoroddsen and Sakakibara (1998). At the initial phase ($t \sim 10$ s), the number of fingers is about 60 with small sizes, as shown in Fig. 4. As the time elapses ($t \sim 30$ s), the number of fingers decreases to ~ 35 and the finger size increases. The number of fingers remains unchanged afterward, as the lamella starts to evaporate and finally dries out.

The threshold of splashing has been correlated with the We and Oh numbers, as well as the ratio of the vertical amplitude of the surface roughness to droplet size (R_{nd}) as follows (Cossali et al. 1997):

$$K_s = We\,Oh^{-0.4} = 649 + 3.76/R_{nd}^{0.63}, \tag{2}$$

where K_s determines the threshold for splashing. According to Table 3, the K numbers associated with the experiments of this work are smaller than K_s obtained from Eq. 2 ($K_s = 4949$ and 4330 for aqueous and IPA-diluted PEDOT:PSS solution droplets, respectively, based on the roughness amplitude of 46 nm and initial droplet sizes given in Table 3) and, thus, no splashing is expected, consistent with the experiments. Having said that, with the high velocity IPA-diluted PEDOT:PSS droplets, a careful inspection of high-speed movies at 10,000 frames/s reveals that, occasionally, secondary droplets may be generated from the finger tips.

4.2.2 Spreading analysis

In the next step, we performed quantitative analysis of droplet spreading ratio $\beta = D/D_0$ versus the dimensionless time $t^* = \frac{tU_0}{D_0}$, as shown in Fig. 5a. The impact dynamics is distinguishable within 3 phases as follows: I: kinematic and spreading; II: relaxation; III: wetting and drying. From Fig. 5a, the temporal evolution of the spreading ratio, $\beta(t^*)$ can be described by two scaling laws, i.e., one purely kinetic in nature $t^{0.5}$ and the other, purely wetting in nature $t^{0.1}$. Spreading dynamics in phase I, strictly follows $\beta(t^*) \propto t^{0.5}$. In phase II, transition of dominant forces started to take place, and entering phase III, pure wetting starts to kick. At the end of phase 3, the maximum, β_{max} and final β_{final} can be determined. To understand the role played by inertia, viscosity, and surface tension, we plotted the β_{max} and β_{final} versus We and Re numbers, shown in Fig. 5b, c, respectively. For aqueous PEDOT:PSS β_{max} and β_{final} scales well with both $We^{0.25}$ and $Re^{0.2}$, reinforcing the notion that their spreading is dominated by inertia. For the IPA-diluted PEDOT:PSS β_{max} and β_{final} show no clear functionality on either We or Re numbers, indicating that inertia, viscous, and capillary forces are all influential in this case. We also observe that in all cases, β_{max} is larger than β_{final} by about 1–2%, indicating only
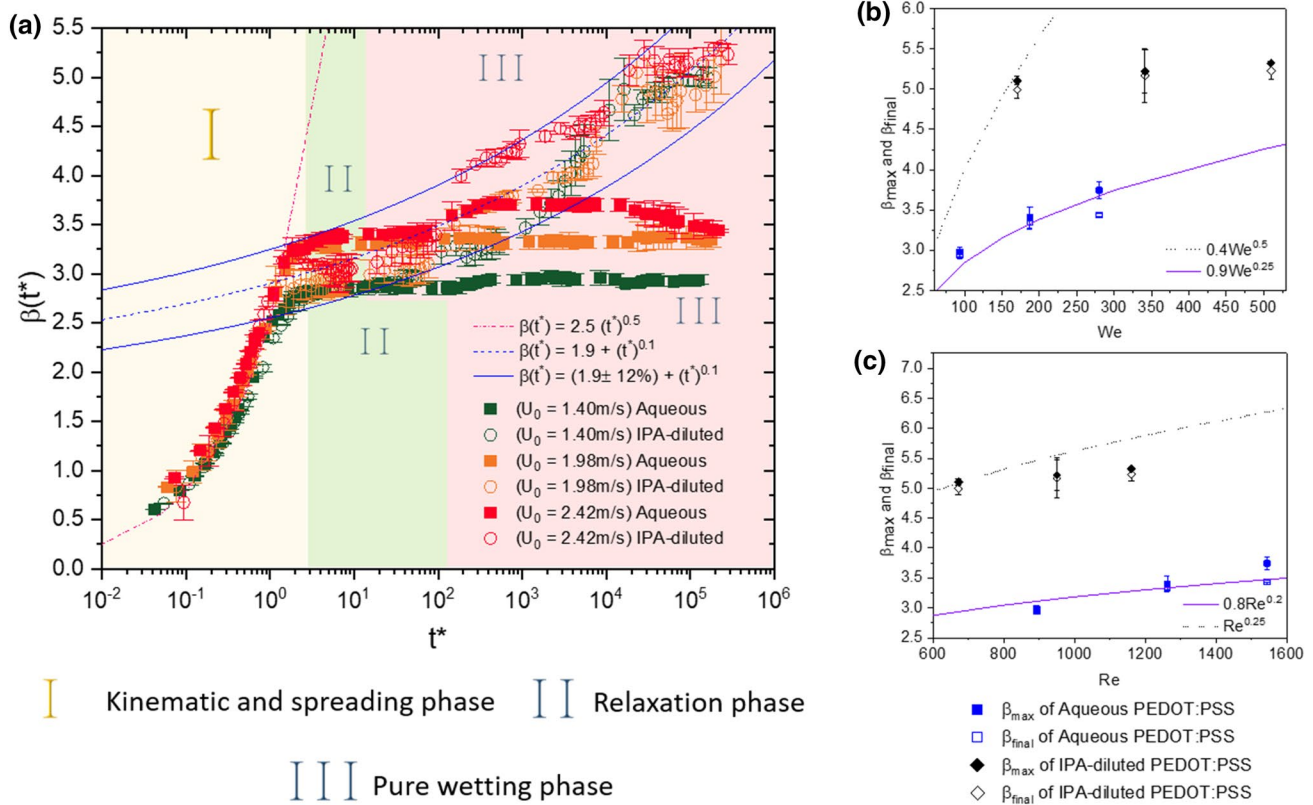
Fig. 5 **a** Temporal evolution of droplet impact dynamics of aqueous and IPA-diluted PEDOT:PSS solution droplets showing three phases. **b** Scaling of β_{max} and β_{final} vs. *We* number. **c** Scaling of β_{max} and β_{final} vs. *Re* number. In **b** and **c**, the closed and open symbols represent β_{max} and β_{final}, respectively. Rectangular and circular symbols denote aqueous and IPA-diluted PEDOT:PSS, respectively. For color interpretation, readers are referred to the online version of this article

a minor retraction. An exception is for the highest velocity impact of the aqueous solution, where an overshooting followed by considerable retraction and shrinkage has occurred, i.e., ~ 8% of β_{max}. Figure 5a shows that at the wetting phase, the aqueous (closed symbols) and IPA-diluted (open symbols) PEDOT:PSS underwent a notoriously different fate, i.e., no further growth for the former, but continuous growth for the latter. To understand what determines their fate, we will discuss the nature of their wettability in the next section.

4.2.3 Role of wettability: dynamic, static, advancing, and receding contact angles

The wettability of the two solutions atop the substrates was studied by analyzing various contact angles of the liquid–substrate system. At early times ($t^* < 1$), the microscopic dynamic contact angle, θ_d, is the most relevant contact angle to look into (Šikalo et al. 2005). When droplet undergoes a transition from the kinematic phase to spreading phase ($t^* \geq 1$), the discussion on macroscopic advancing, θ_a, and receding, θ_r, contact angles becomes necessary (Fukai

et al. 1995; Yokoi et al. 2009). At later times ($t^* \gg 1$), the process is extremely slow or virtually in equilibrium, and wettability can be characterized in terms of quasi-static contact angle, θ_s.

We measured the θ_d of two solution droplets for three different impinging velocities. Measurements were performed at the triple line, from the magnified images, started right after the droplet impinged upon the surface up to the point of transition from kinematic to spreading phase (i.e., $t^* \geq 1$) (Fig. 6). The θ_d is indeed dynamic and fluctuates with time, and gradually decreases as the droplet enters the relaxation and wetting phases. In Fig. 6, we can identify a clear distinction in trend between aqueous and IPA-diluted PEDOT:PSS solution droplets. Throughout the rapid kinematic spreading phase (cf. phase I of Fig. 5), the latter attain a much larger θ_d relative to the former. This can be attributed to the smaller viscous force of the IPA-diluted PEDOT:PSS, especially at the vicinity of the triple line. A detailed study regarding the link between θ_d, U_{cl}, and flow at the moving contact line can be found in Šikalo et al. (2005).

Once the dynamic fluctuations damp out, i.e., at the end of the spreading stage, we can define the two limiting contact
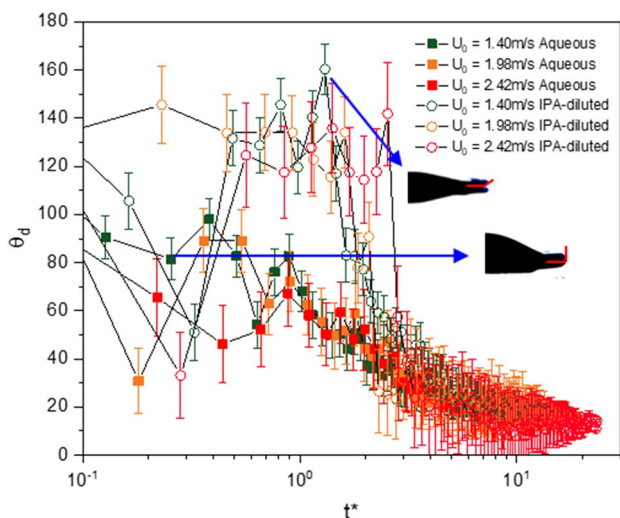
Fig. 6 Temporal evolution of dynamic contact angle, θ_d in degrees, for aqueous and IPA-diluted PEDOT:PSS droplets on FTO-coated glass substrate

angles θ_a and θ_r, the advancing and receding contact angles, respectively. The value of quasi-static contact angle, θ_s, or sometimes referred to as apparent contact angle, should then fall between the aforementioned two values. The values for these contact angles are presented in Table 5.

For aqueous PEDOT:PSS, $\theta_s = 17.6° \pm 1.2°$, representing a partially wetting system. For IPA-diluted PEDOT:PSS, right after the droplet touchdown, we observe that there is a state where contact angle remains stable for a brief period (~ 1 s), creating a plateau, then droplet continues to spread to reach ~ 0, i.e., a complete wetting system. To understand this "momentarily pause", we adopt an average contact angle introduced by Villa et al. (2018) during this brief plateau stage, measured as $10.2° \pm 2.5°$. Interestingly, the beginning and the end of the plateau stage of this momentarily pause correspond precisely to time span of the phase II in Fig. 5a (relaxation phase). This suggests that the plateau stage is the transition phase from kinematic spreading to a spreading increasingly dominated by wetting. After this momentary pinning, the contact angle decays over time, with rate following $\theta(t) \propto t^{-0.3}$ predicted by tanner for a fully wetting system (Tanner 1979) and eventually reaches $\sim 0°$.

Table 5 Advancing (θ_a), receding (θ_r), and static (θ_s) contact angles of aqueous and IPA-diluted PEDOT:PSS solution droplets on FTO-coated glass substrate

Solution	θ_a (°)	θ_r (°)	θ_s (°)
Aqueous PEDOT:PSS	24.4 ± 2.7	6.2 ± 1.5	17.6 ± 1.2
IPA-diluted PEDOT:PSS	19.8 ± 3.5	–	–

4.2.4 Spreading prediction models

Figure 7 shows the predicted β_{max} using model Eqs. S1–S7 compared with our experimental results. When required, the static contact angle, θ_s, was used in the model equations. For aqueous PEDOT:PSS droplets, most models predict the experimental with an error of < 10%, as Fig. 7 shows. For the IPA-diluted PEDOT:PSS droplets, the disagreement was larger due to the presence of dominantly wetting phase of the latter droplets. On account of the wetting phase and its effect on spreading, we included the Tanner's law in the dimensionless form, $(t^*)^{0.1}$, arriving at a family of modified correlations for a fully wetting system, in the form:

$$\beta_{max} = f\left(Re, We, \theta_s\right) + (t^*)^{0.1} \qquad (3)$$

where the first and second terms on the right-hand side can be any existing correlation (Eqns. S1-S7 of the SI) and the Tanner's law for spreading in the wetting phase, respectively. t^* corresponds to the lifetime of the spread before it starts to evaporate, here ~ 300 s. Spreading behavior in the form of Eq. (3) has been previously observed by Rioboo et al. (2002), as well. In principle, for a fully wetting system, the time t^* in the term $(t^*)^{0.1}$, discussed above, could extend indefinitely, if drying and evaporation are neglected, i.e., a continuous wetting process with infinitely decaying rate may take place. This issue had been addressed by De Gennes (1985), where he proposed that such wetting would
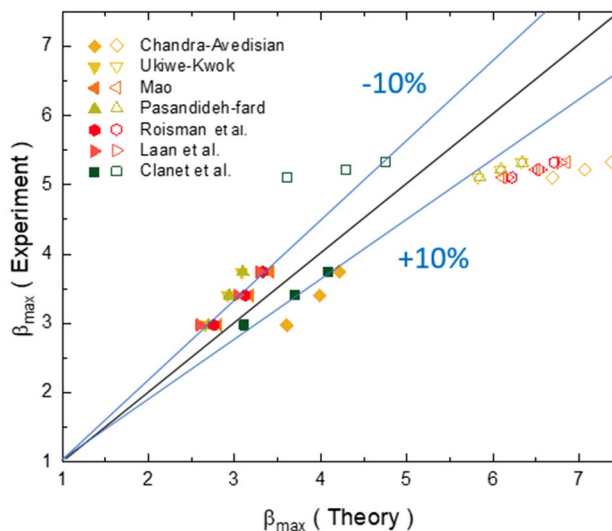
Fig. 7 Comparison of experimental data and models prediction for β_{max}. Closed and open symbols represent aqueous and IPA-diluted PEDOT:PSS solution droplets, respectively. For aqueous PEDOT:PSS droplet, proposed model equations (Eq. S1–S7 of the SI) were used, whereas for the IPA-diluted PEDOT:PSS droplets, a wetting stage was added to the existing correlations and our modified Eq. (3) was used

go on to form a presumably one single-molecule thick film. In real situations, such spreading has also been observed by many, prominently by Benjamin Franklin infamous experiments (Benjamin et al. 1774), where for one teaspoon of olive oil ($\sim 2 \times 10^{-6}$ m^3) dropped on the water surface, an oil layer of roughly 2213 m^2 forms. This implies a thickness of 10×10^{-10} m or 1 nm. Olive oil has $\sigma \sim 30$ mN/m (Sahasrabudhe et al. 2017) and for water, we have $\sigma = 72.8$ mN/m. The above system is comparable to what we have in this study, with $\sigma = 25$ mN/m for the IPA-diluted solution, and $\sigma_{sv} = 80$ mN/m for the FTO-coated glass substrate.

For IPA-diluted PEDOT:PSS droplet, the modified predictions show discrepancy that vary between ~ 15 and 35%, as shown in Fig. 7. We attribute this to the influence of the dynamic contact angle, whereas the model correlations use a static contact angle, reproducibility of experiment data ($< 6\%$), and complex nature of IPA-diluted PEDOT:PSS solution, which is a composite solution with shear-thinning behavior. We investigated how the variation of contact angle affects the accuracy of prediction models for maximum spreading, by varying the contact angle from 0° to 180°, where variations of ± 1–5% in prediction of β_{max} were observed.

4.3 Impact dynamics and coalescence of multiple droplets

In coating and printing applications, such as inkjet printing and spray coating, multiple droplets impact a substrate to produce a line or film. When multiple droplets are deposited, the neighboring droplets may undergo coalescence, depending on the spreading extend and droplet spacing. In our experiments, the droplet release spacing was fixed on 10 mm, which assured coalescence in most cases, for the droplet size and the range of β_{max} obtained for a single droplet, studied in Sect. 4.2. The center-to-center drop spacing after landing (δ) deviated slightly from the fixed initial launch spacing of 10 mm, with the amount of 10.5 mm $\pm$ 0.7 mm, $\sim 7\%$ maximum deviation from the mean value.

The typical coalescence of two droplets is shown in Fig. 8, where the early dynamics phase and late wetting evolution phase of the process are shown. More examples are provided in Figures S5–S8 of the SI, for two and five impinged droplets. Out of the six cases studied here, only aqueous PEDOT:PSS with lowest impact velocity did not result in coalescence, as shown in Fig. 8. The figure reveals a scalloped (partial) coalescence (left column, $U_0 = 1.98$ m/s and $U_0 = 2.42$ m/s) and a complete coalescence (right column). The scalloped pattern may form due to two reasons: excessive spacing and/or insufficient driving force for coalescence. Thus, based on Fig. 8 and other supporting images, we identified that the coalescence could be either direct or
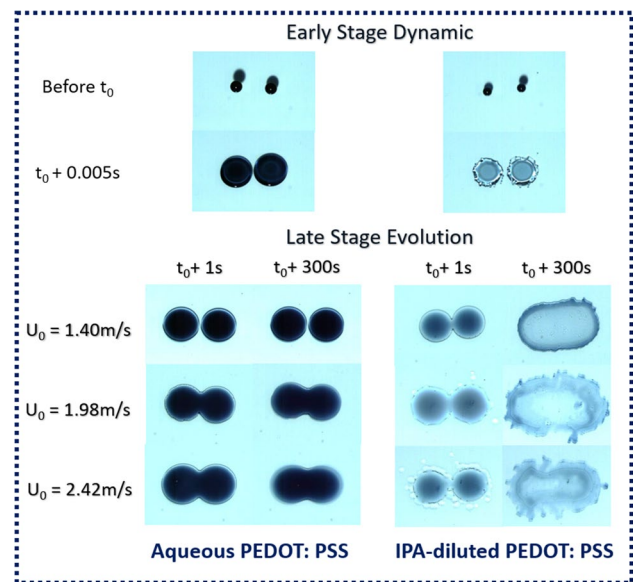
Fig. 8 Early dynamic and late evolution phases of two coalescing droplets of aqueous (left column) and IPA-diluted (right column) PEDOT:PSS solutions. In-flight droplet size is ~ 3.3 mm and ~ 2.6 mm for aqueous and IPA-diluted PEDOT:PSS, respectively, and t_0 is the time of impact

indirect. A direct coalescence occurs if both droplets are still in the kinematic spreading phase, while an indirect coalescence occurs only after the two droplets have entered the slow wetting stage. Here, the aqueous PEDOT:PSS droplet represents the typical direct coalescence, whereas the smaller IPA-diluted PEDOT:PSS droplet is a paragon of indirect coalescence, as the coalescence only happens after the droplets have entered the wetting stage. From a practical point of view, and particularly if the substrate is heated or solvent evaporation is fast, direct coalescence is advantageous for achieving a more smooth and uniform coating, otherwise a stacked-coin pattern may form.

The coalescence process begins upon contact between the boundaries of the two droplets, forming a bridge. The distinction between different possible coalescence states is illustrated in Fig. 9a, with two cases of partial coalescence $L_b \ll D_s$ and $L_b < D_s$ and one case of full coalescence, $L_b \geq D_s$, where L_b is the bridge length and D_s is the diameter of an individual growing spread. Upon impact, the coalescence is dominated by the droplet inertia or kinetic energy. In this regime, the bridge growth follows a power law in the form $L_b \propto t^{0.5}$ (Eggers et al. 1999). Figure 9b shows excellent agreement between the experimental data for both aqueous and IPA-diluted PEDOT:PSS droplets and the aforementioned power law, also shown on the figure. It is noted that in a viscosity-dominant setting, the scaling law is in the form of $L_b \propto t^{0.25}$, as proposed by Lee et al. (2012). After the kinematic phase, the growth of the bridge length slows down and follows either a Tanner's law dependency
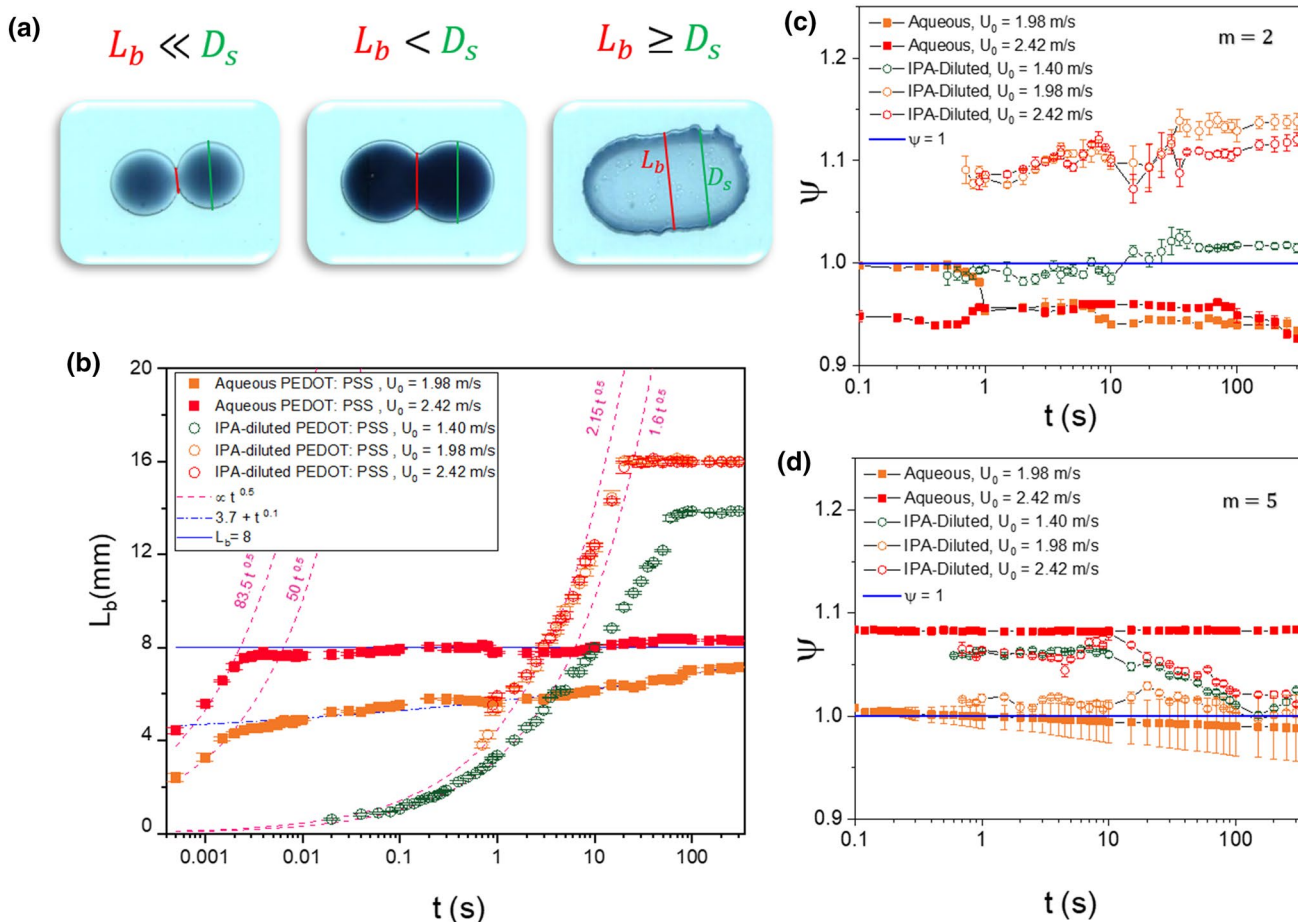
Fig. 9 **a** Several possible coalescence scenarios. **b** Temporal growth of L_b between two coalescing droplets, **c** and **d** temporal evolution of dimensionless spread length ψ of multiple droplets in an array with number of droplets, $m = 2$ and 5, respectively. In **b**, the shown pink dashed-line curves fit the experimental data in the kinematic phase, consistent with analysis of Eggers et al. (1999) ($L_b \propto t^{0.5}$). In the wetting phase, the unpinned cases follow the Tanner's law growth $L_b \propto t^{0.1}$, whereas the growth of the pinned cases stops ($L_b = 8$)
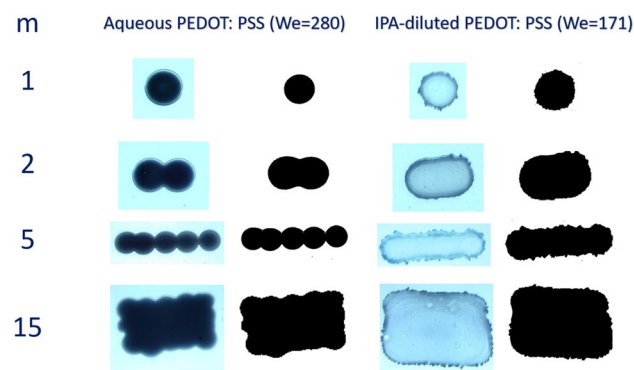
($L_b \propto t^{0.1}$), when pinning does not occur prior to drying or growth stops, when the droplets are pinned, as presented in Fig. 9b. In a different setting, coalescence and bridging of resin solution droplets in large timescales in the wetting phase were studied, where a similar timescale was observed, i.e., $L_b \propto t^{0.1}$ (Yarin et al., 2019).

As the time elapses, kinetic energy is dissipated and eventually the bridge growth stops as contact line pinning occurs. Li et al. (2010) evaluated the ideality of the growth process by defining a dimensionless time-dependent spread length $\psi = \frac{D_y}{D_s + \delta}$, where D_y is the spread length along the abscissa direction and D_s is the spread length/diameter of a single droplet in the ordinate direction, as depicted in the graphical abstract. Thus, ψ is the ratio of actual spread length to the spread length of an individual droplet plus the center-to-center spacing between the two droplets. Based on their definition, when $\psi < 1$, less than ideal spreading occurs, called drawback by Li et al. (2010), whereas when $\psi > 1$,

additional spreading is attained. Using the spreading data of the single droplet impact obtained in Sect. 4.2 for D_s and data of this section for multiple droplets for D_y, the temporal evolution of ψ for all coalescence cases for two and five droplets is presented in Fig. 9c, d, respectively. Coalescence of two droplets of aqueous PEDOT:PSS exhibits a spreading length that is less than ideal, i.e., $\psi < 1$ (Fig. 9c). This behavior is a further manifestation of the overshooting and receding associated with this solution, as discussed in the previous section. However, when the number of droplets, m, along the array is increased, here from 2 to 5, the ratio of D_y/D_s becomes increasingly larger. Thus, receding happens at the contact line of the two outermost droplets only, no longer affecting the overall D_y and ψ. Hence, ψ could become larger than 1 (Fig. 9d) and this tendency is more pronounced, as the impact velocity increases. Thus, increasing the number of multiple droplets improves the ideality of the coating. On the other hand, for IPA-diluted PEDOT:PSS, whose coalescence is indirect and receding is absent, $\psi > 1$ when

$m = 2$. However, edge instabilities decrease as m increases, because the ratio of perimeter with respect to coating area decreases as m increases, leading to less irregular instability. This results in a decrease in ψ, while still $\psi > 1$.

Here, we define another kind of ideality for the coating process, depending on the number of droplets, m, and how the droplets are arranged to form a line or film. Figure 10 exhibits typical relation between the number of droplets and the shape of the ensuing line or film. For a single droplet, we have an explicit circular ideality. For multiple droplets, ideality depends on the purpose of printing, which is usually to achieve rectangular lines or films with high regularity and resolution. Thus, the ideal surface area is the maximum area that can be filled by multiple impinging droplets at a given droplet spacing and spreading of an individual droplet. Here for $m = 1$, we applied a circular ideality and for $m = 2$, 5 and 15, the rectangular ideality was applied for both solutions. The equations to calculate the proposed ideal surface areas are listed in Table 6. The comparison between quantified actual surface area versus the ideal surface is presented in Fig. 11. A less than ideal surface area often occurs due to non-coalescence or partial coalescence situation, generally, due to over spacing, or under spreading; thus, in these cases, reducing the droplet-to-droplet spacing can improve the film quality. Increasing the impact velocity also improves spreading and, therefore, droplet coalescence and film ideality as depicted in Fig. 11, provided that increased velocity does not result in splashing and increased irregularities at the boundaries. A higher than ideal surface area observed in IPA-diluted droplets, as shown in Fig. 11, is due to irregular spreading and instabilities at the edges, which has resulted in additional but irregular surface area (higher surface area but insufficient resolution). It is worth nothing that the ideality of the coating also depends on homogeneity of the film, i.e., uniform distribution of the coating material in the film. While beyond the scope of this work, it appears that the
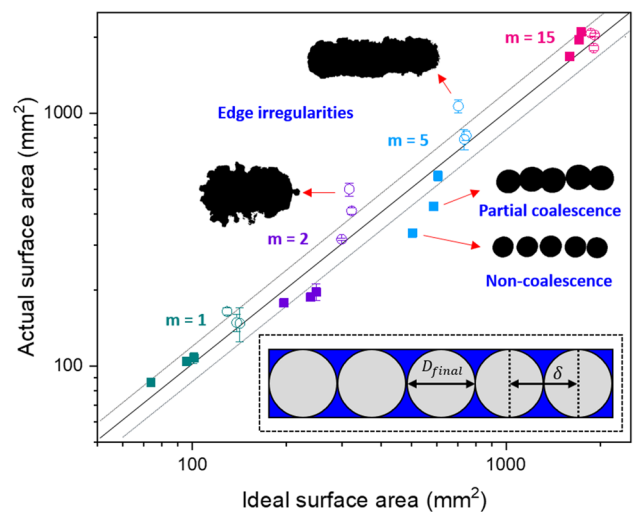
Table 6 Equations of relevant ideal circular or rectangular areas, where D_{final} is the final spread diameter of a single droplet and δ is the center-to-center droplet spacing

No. of droplets/type of ideality	Ideal surface area (A)
1/circular dot	$\pi(D_{final}/2)^2$
2/rectangular line	$(D_{final} + \delta)(D_{final})$
5/rectangular line	$(D_{final} + 4\delta)(D_{final})$
15/rectangular film	$(4\delta + D_{final})(2\delta + D_{final})$

addition of IPA may have resulted in some degree of separation of components of IPA-diluted PEDOT:PSS solution. To improve mixing and to increase droplet spreading, Eslamian and Soltani-Kordshuli (2018) suggested to impose ultrasonic vibrations on the substrate.

5 Conclusions

In summary, we analyzed the impact dynamics of single and multiple aqueous and IPA-diluted PEDOT:PSS droplets, impinged on FTO-coated glass substrate, nearly simultaneously for multiple droplets impact. The role of various contact angles, from dynamic to static, during spreading was studied, where we found stochastic behavior in dynamic contact angles in the kinematic phase, but eventually the contact angles reached a static value in the relaxation phase.

Fig. 10 Actual and binarized images used for extracting the actual surface area of the formed pattern. The single droplets splat is ~12 and ~14 mm for the aqueous and IPA-diluted PEDOT:PSS droplets, respectively

Fig. 11 The ideal vs. actual scaling behavior of coalescing multiple droplets. Solid rectangular symbols represent aqueous PEDOT:PSS solution and open circle symbols are for IPA-diluted PEDOT:PSS. For color interpretation related to the number of droplets, m, readers are referred to the online version of this paper. Dotted lines represent $\pm 20\%$ deviations. The inset illustrates the definition of the ideal surface area for $m = 5$. D_{final} is final diameter of a single spreading droplet, and δ is the center-to-center drop spacing

For aqueous PEDOT:PSS solution, the static contact angle was 17.6°, forming a partially wetting system with the substrate. Existing correlations for spreading were able to predict the spreading of this solution. On the other hand, for the IPA-diluted PEDOT:PSS solution, the static contact angle was near zero, creating a fully wetting system with the substrate. This resulted in substantial additional spreading in the prolonged wetting phase following the Tanner's power law based on dimensionless time. The total spreading for such a fully wetting system was fairly predicted using existing correlations for maximum spreading in the dynamic phase plus additional spreading using Tanner's law in the wetting phase (Eq. 3). Thus, the spreading of liquids that fully wet the surface, such as IPA-diluted PEDOT:PSS solution is best described using Eq. 3. We also examined the bridge formation, spread length growth, and shape evolution of multiple coalescing droplets. Furthermore, we demonstrated a scaling linearity for surface area vs the number of droplets for systems of multiple coalescing droplets, up to 15 droplets forming a coating. The droplet center-to-center spacing, a geometrical parameter, as well as individual droplet spreading behavior governed by *We* and *Re* numbers control the ideal surface area of the final coating. For a given spacing and spreading, the ideal surface areas for multiple droplets were provided and compared with the experimental values.

Author contributions DB and ME devised the project. DB performed the experiments and analyses, prepared the figures and drafted the manuscript. ME revised the manuscript and improved the interpretation of the results. ME conceived and outlined the project direction and objectives and secured research funding.

Compliance with ethical standards

Conflict of interest The authors declare no competing interests.

References

Aarts DGAL, Lekkerkerker HNW, Guo H et al (2005) Hydrodynamics of droplet coalescence. Phys Rev Lett 95:164503. https://doi.org/10.1103/PhysRevLett.95.164503

Andrade R, Skurtys O, Osorio F (2015) Development of a new method to predict the maximum spread factor for shear thinning drops. J Food Eng 157:70–76. https://doi.org/10.1016/j.jfoodeng.2015.02.017

Andrieu C, Beysens DA, Nikolayev VS, Pomeau Y (2002) Coalescence of sessile drops. J Fluid Mech 453:427–438. https://doi.org/10.1017/S0022112001007121

Antonini C, Amirfazli A, Marengo M (2012) Drop impact and wettability: from hydrophilic to superhydrophobic surfaces. Phys Fluids 24:102104. https://doi.org/10.1063/1.4757122

Ashoke Raman K, Jaiman RK, Lee T-S, Low H-T (2017) Dynamics of simultaneously impinging drops on a dry surface: role of impact velocity and air inertia. J Colloid Interface Sci 486:265–276. https://doi.org/10.1016/j.jcis.2016.09.062

Bartolo D, Boudaoud A, Narcy G, Bonn D (2007) Dynamics of Non-Newtonian droplets. Phys Rev Lett 99:174502. https://doi.org/10.1103/PhysRevLett.99.174502

Benjamin F, William B, Null F (1774) XLIV. Of the stilling of waves by means of oil. Extracted from sundry letters between Benjamin Franklin, LL. D. F. R. S. William Brownrigg, M. D. F. R. S. and the Reverend Mr. Farish. Philos Trans R Soc Lond 64:445–460. https://doi.org/10.1098/rstl.1774.0044

Bertola V (2013) Dynamic wetting of dilute polymer solutions: the case of impacting droplets. Adv Colloid Interface Sci 193–194:1–11. https://doi.org/10.1016/j.cis.2013.03.001

Biance A-L, Clanet C, Quéré D (2004) First steps in the spreading of a liquid droplet. Phys Rev E Stat Nonlinear Soft Matter Phys 69:163011–163014

Brian D, Ahmadian-Yazdi M-R, Barratt C, Eslamian M (2019) Impact dynamics and deposition of perovskite droplets on PEDOT:PSS and TiO2 coated glass substrates. Exp Therm Fluid Sci 105:181–190. https://doi.org/10.1016/j.expthermflusci.2019.03.021

Castrejón-Pita JR, Kubiak KJ, Castrejón-Pita AA et al (2013) Mixing and internal dynamics of droplets impacting and coalescing on a solid surface. Phys Rev E Stat Nonlinear Soft Matter Phys 88:023023. https://doi.org/10.1103/PhysRevE.88.023023

Chandra S, Avedisian CT (1991) On the collision of a droplet with a solid surface. Proc R Soc A Math Phys Eng Sci 432:13–41. https://doi.org/10.1098/rspa.1991.0002

Cira NJ, Benusiglio A, Prakash M (2015) Vapour-mediated sensing and motility in two-component droplets. Nature 519:446

Clanet C, Béguin C, Richard D, Quéré D (2004) Maximal deformation of an impacting drop. J Fluid Mech 517:199–208. https://doi.org/10.1017/S0022112004000904

Cooper-White JJ, Crooks RC, Chockalingam K, Boger DV (2002) Dynamics of polymer-surfactant complexes: elongational properties and drop impact behavior. Ind Eng Chem Res 41:6443–6459. https://doi.org/10.1021/ie020001v

Cossali GE, Coghe A, Marengo M (1997) The impact of a single drop on a wetted solid surface. Exp Fluids 22:463–472. https://doi.org/10.1007/s003480050073

De Gennes PG (1985) Wetting: statics and dynamics. Rev Mod Phys 57:827–863. https://doi.org/10.1103/RevModPhys.57.827

Derby B (2010) Inkjet printing of functional and structural materials: fluid property requirements, feature stability, and resolution. Annu Rev Mater Res 40:395–414. https://doi.org/10.1146/annurev-matsci-070909-104502

Duchemin L, Eggers J, Josserand C (2003) Inviscid coalescence of drops. J Fluid Mech 487:167–178. https://doi.org/10.1017/S0022112003004646

Duineveld PC (2003) The stability of ink-jet printed lines of liquid with zero receding contact angle on a homogeneous substrate. J Fluid Mech. https://doi.org/10.1017/s0022112002003117

Eddi A, Winkels KG, Snoeijer JH (2013) Influence of droplet geometry on the coalescence of low viscosity drops. Phys Rev Lett. https://doi.org/10.1103/physrevlett.111.144502

Eggers J, Lister JR, Stone HA (1999) Coalescence of liquid drops. J Fluid Mech 401:293–310. https://doi.org/10.1017/S002211209900662X

Eggers J, Fontelos MA, Josserand C, Zaleski S (2010) Drop dynamics after impact on a solid wall: theory and simulations. Phys Fluids 22:062101. https://doi.org/10.1063/1.3432498

Elschner A, Kirchmeyer S, Lövenich W et al (2010) PEDOT: Principles and applications of an intrinsically conductive polymer. CRC Press, Boca Raton. https://doi.org/10.1201/b10318

Eom SH, Senthilarasu S, Uthirakumar P et al (2009) Polymer solar cells based on inkjet-printed PEDOT:PSS layer. Org Electron Phys Mater Appl 10:536–542. https://doi.org/10.1016/j.orgel.2009.01.015

Eslamian M (2013) A mathematical model for the design and fabrication of polymer solar cells by spray coating. Dry Technol 31:405–413. https://doi.org/10.1080/07373937.2012.737397

Eslamian M (2014) Spray-on thin film PV solar cells: advances, potentials and challenges. Coatings 4:60–84. https://doi.org/10.3390/coatings4010060

Eslamian M (2017) Inorganic and organic solution-processed thin film devices. Nano Micro Lett 9:3. https://doi.org/10.1007/s40820-016-0106-4

Eslamian M, Soltani-Kordshuli F (2018) Development of multiple-droplet drop-casting method for the fabrication of coatings and thin solid films. J Coat Technol Res 15:271–280. https://doi.org/10.1007/s11998-017-9975-9

Finotello G, De S, Vrouwenvelder JCR et al (2018) Experimental investigation of non-Newtonian droplet collisions: the role of extensional viscosity. Exp Fluids 59:113. https://doi.org/10.1007/s00348-018-2568-2

Fukai J, Shiiba Y, Yamamoto T et al (1995) Wetting effects on the spreading of a liquid droplet colliding with a flat surface: experiment and modeling. Phys Fluids 7:236–247. https://doi.org/10.1063/1.868622

German G, Bertola V (2009) Impact of shear-thinning and yield-stress drops on solid substrates. J Phys Condens Matter 21:37. https://doi.org/10.1088/0953-8984/21/37/375111

Gudapati H, Dey M, Ozbolat I (2016) A comprehensive review on droplet-based bioprinting: past, present and future. Biomaterials 102:20–42. https://doi.org/10.1016/j.biomaterials.2016.06.012

Hernández-Sánchez JF, Lubbers LA, Eddi A, Snoeijer JH (2012) Symmetric and asymmetric coalescence of drops on a substrate. Phys Rev Lett 109:184502. https://doi.org/10.1103/PhysRevLett.109.184502

Hoath SD, Jung S, Hsiao W-K, Hutchings IM (2012) How PEDOT:PSS solutions produce satellite-free inkjets. Org Electron Phys Mater Appl 13:3259–3262. https://doi.org/10.1016/j.orgel.2012.10.004

Hoth CN, Choulis SA, Schilinsky P, Brabec CJ (2007) High photovoltaic performance of inkjet printed polymer: fullerene blends. Adv Mater 19:3973–3978. https://doi.org/10.1002/adma.200700911

Josserand C, Thoroddsen ST (2016) Drop impact on a solid surface. Annu Rev Fluid Mech 48:365–391

Laan N, De Bruin KG, Bartolo D et al (2014) Maximum diameter of impacting liquid droplets. Phys Rev Appl 2:044018. https://doi.org/10.1103/PhysRevApplied.2.044018

Lee MW, Kang DK, Yoon SS, Yarin AL (2012) Coalescence of two drops on partially wettable substrates. Langmuir 28:3791–3798. https://doi.org/10.1021/la204867c

Lee MW, Kim NY, Chandra S, Yoon SS (2013) Coalescence of sessile droplets of varying viscosities for line printing. Int J Multiph Flow 56:138–148. https://doi.org/10.1016/j.ijmultiphaseflow.2013.06.004

Li R, Ashgriz N, Chandra S et al (2010) Coalescence of two droplets impacting a solid surface. Exp Fluids 48:1025–1035. https://doi.org/10.1007/s00348-009-0789-0

Liu Y, Tan P, Xu L (2015) Kelvin–Helmholtz instability in an ultrathin air film causes drop splashing on smooth surfaces. Proc Natl Acad Sci 112:3280–3284. https://doi.org/10.1073/pnas.1417718112

Mahajan A, Frisbie CD, Francis LF (2013) Optimization of aerosol jet printing for high-resolution, high-aspect ratio silver lines. ACS Appl Mater Interfaces 5:4856–4864. https://doi.org/10.1021/am400606y

Mao T, Kuhn DCS, Tran H (1997) Spread and rebound of liquid droplets upon impact on flat surfaces. AIChE J 43:2169–2179. https://doi.org/10.1002/aic.690430903

Marmanis H, Thoroddsen ST (1996) Scaling of the fingering pattern of an impacting drop. Phys Fluids 8:1344–1346. https://doi.org/10.1063/1.868941

McCoul D, Rosset S, Schlatter S, Shea H (2017) Inkjet 3D printing of UV and thermal cure silicone elastomers for dielectric elastomer actuators. Smart Mater Struct 26:125022. https://doi.org/10.1088/1361-665x/aa9695

Menchaca-Rocha A, Martínez-Dávalos A, Núñez R (2001) Coalescence of liquid drops by surface tension. Phys Rev E Stat Phys Plasmas Fluids Relat Interdiscip Top 63:046309. https://doi.org/10.1103/PhysRevE.63.046309

Narhe R, Beysens D, Nikolayev VS (2004) Contact line dynamics in drop coalescence and spreading. Langmuir 20:1213–1221. https://doi.org/10.1021/la034991g

Ouyang J, Chu C-W, Chen F-C et al (2005) High-conductivity poly(3,4-ethylenedioxythiophene):poly(styrene sulfonate) film and its application in polymer optoelectronic devices. Adv Funct Mater 15:203–208. https://doi.org/10.1002/adfm.200400016

Pasandideh-Fard M, Qiao YM, Chandra S, Mostaghimi J (1996) Capillary effects during droplet impact on a solid surface. Phys Fluids 8:650–659. https://doi.org/10.1063/1.868850

Paulsen JD, Burton JC, Nagel SR (2011) Viscous to inertial crossover in liquid drop coalescence. Phys Rev Lett 106:114501. https://doi.org/10.1103/PhysRevLett.106.114501

Rein M, Delplanque J-P (2008) The role of air entrainment on the outcome of drop impact on a solid surface. Acta Mech 201:105. https://doi.org/10.1007/s00707-008-0076-9

Rioboo R, Tropea C, Marengo M (2001) Outcomes from a drop impact on solid surfaces. At Sprays 11:155–165

Rioboo R, Marengo M, Tropea C (2002) Time evolution of liquid drop impact onto solid, dry surfaces. Exp Fluids 33:112–124. https://doi.org/10.1007/s00348-002-0431-x

Ristenpart WD, McCalla PM, Roy RV, Stone HA (2006) Coalescence of spreading droplets on a wettable substrate. Phys Rev Lett 97:064501. https://doi.org/10.1103/PhysRevLett.97.064501

Rivadeneyra A, Bobinger M, Albrecht A et al (2019) Cost-effective PEDOT:PSS temperature sensors Inkjetted on a bendable substrate by a consumer printer. Polymers 11:5

Roisman IV (2009) Inertia dominated drop collisions. II. An analytical solution of the Navier-Stokes equations for a spreading viscous film. Phys Fluids 21:052104. https://doi.org/10.1063/1.3129283

Roisman IV, Berberović E, Tropea C (2009) Inertia dominated drop collisions. I. On the universal flow in the lamella. Phys Fluids 21:052103. https://doi.org/10.1063/1.3129282

Sahasrabudhe SN, Rodriguez-Martinez V, O'Meara M, Farkas BE (2017) Density, viscosity, and surface tension of five vegetable oils at elevated temperatures: measurement and modeling. Int J Food Prop 20:1965–1981. https://doi.org/10.1080/10942912.2017.1360905

Sarojini Kg K, Dhar P, Varughese S, Das SK (2016) Coalescence dynamics of PEDOT:PSS droplets impacting at offset on substrates for Inkjet printing. Langmuir 32:5838–5851. https://doi.org/10.1021/acs.langmuir.6b01219

Scheller BL, Bousfield DW (1995) Newtonian drop impact with a solid surface. AIChE J 41:1357–1367. https://doi.org/10.1002/aic.690410602

Schiaffino S, Sonin AA (1997) Molten droplet deposition and solidification at low Weber numbers. Phys Fluids 9:3172–3187. https://doi.org/10.1063/1.869434

Šikalo Š, Wilhelm H-D, Roisman IV et al (2005) Dynamic contact angle of spreading droplets: experiments and simulations. Phys Fluids 17:1–13. https://doi.org/10.1063/1.1928828

Soltani-Kordshuli F, Eslamian M (2017) Impact dynamics and deposition of pristine and graphene-doped PEDOT:PSS polymeric droplets on stationary and vibrating substrates. Exp Therm Fluid Sci 89:238–248. https://doi.org/10.1016/j.expthermflusci.2017.08.019

Tanner LH (1979) The spreading of silicone oil drops on horizontal surfaces. J Phys D Appl Phys 12:1473–1484. https://doi.org/10.1088/0022-3727/12/9/009

Thoroddsen ST, Sakakibara J (1998) Evolution of the fingering pattern of an impacting drop. Phys Fluids 10:1359–1374. https://doi.org/10.1063/1.869661

Thoroddsen ST, Takehara K, Etoh TG (2005) The coalescence speed of a pendent and a sessile drop. J Fluid Mech 527:85–114. https://doi.org/10.1017/S0022112004003076

Thoroddsen ST, Qian B, Etoh TG, Takehara K (2007) The initial coalescence of miscible drops. Phys Fluids 19:072110. https://doi.org/10.1063/1.2746382

Torrisi F, Hasan T, Wu W et al (2012) Inkjet-printed graphene electronics. ACS Nano 6:2992–3006. https://doi.org/10.1021/nn2044609

Ukiwe C, Kwok DY (2005) On the maximum spreading diameter of impacting droplets on well-prepared solid surfaces. Langmuir 21:666–673. https://doi.org/10.1021/la0481288

Villa F, Marengo M, De Coninck J (2018) A new model to predict the influence of surface temperature on contact angle. Sci Rep 8:6549. https://doi.org/10.1038/s41598-018-24828-8

Wang T, Derby B (2005) Ink-Jet printing and sintering of PZT. J Am Ceram Soc 88:2053–2058. https://doi.org/10.1111/j.1551-2916.2005.00406.x

Wijshoff H (2018) Drop dynamics in the inkjet printing process. Curr Opin Colloid Interface Sci 36:20–27. https://doi.org/10.1016/j.cocis.2017.11.004

Wu M, Cubaud T, Ho C-M (2004) Scaling law in liquid drop coalescence driven by surface tension. Phys Fluids 16:L51–L54. https://doi.org/10.1063/1.1756928

Xu L (2010) Instability development of a viscous liquid drop impacting a smooth substrate. Phys Rev E 82:25303. https://doi.org/10.1103/PhysRevE.82.025303

Yarin AL (2006) Drop impact dynamics: splashing, spreading, receding, bouncing. Annu Rev Fluid Mech 38:159–192

Yarin AL, Weiss DA (1995) Impact of drops on solid surfaces: self-similar capillary waves, and splashing as a new type of kinematic discontinuity. J Fluid Mech 283:141–173. https://doi.org/10.1017/S0022112095002266

Yarin AL, Lee MW, An S, Yoon SS (2019) Chapter 3 of "Self-Healing Nanotextured Vascular Engineering Materials". Springer Nature, Basel, pp 37–55. https://doi.org/10.1007/978-3-030-05267-6

Yokoi K, Vadillo D, Hinch J, Hutchings I (2009) Numerical studies of the influence of the dynamic contact angle on a droplet impacting on a dry surface. Phys Fluids 21:072102. https://doi.org/10.1063/1.3158468

Zabihi F, Xie Y, Gao S, Eslamian M (2015) Morphology, conductivity, and wetting characteristics of PEDOT:PSS thin films deposited by spin and spray coating. Appl Surf Sci 338:163–177. https://doi.org/10.1016/j.apsusc.2015.02.128

Affiliations

Dominikus Brian[1] · Morteza Eslamian[1]

✉ Morteza Eslamian
Morteza.Eslamian@sjtu.edu.cn;
Morteza.Eslamian@gmail.com

1   University of Michigan-Shanghai Jiao Tong University Joint Institute, Shanghai 200240, China